Energy & Environmental Science

RSC Publishing

ANALYSIS

View Article Online
View Journal | View Issue

Cite this: *Energy Environ. Sci.*, 2013, **6**, 2561

$ per W metrics for thermoelectric power generation: beyond *ZT*†

Shannon K. Yee,*[a] Saniya LeBlanc,[bc] Kenneth E. Goodson[b] and Chris Dames*[a]

Thermoelectric materials for power generation are typically compared using the dimensionless figure-of-merit *ZT* because it relates directly to the device efficiency. However, for practical applications, the cost of power generation – as governed by material, manufacturing, and heat exchanger costs – is also a critical factor which is not captured in *ZT* alone. The necessary analysis, derived herein, optimizes the coupled thermoelectric and economic problem for the leg length, *L*, and system fill factor, *F*, as functions of these costs. Fuel, operating, and maintenance costs are excluded. This optimization yields the minimum $ per W value for thermoelectric power generation and a framework for comparing materials beyond *ZT*. This analysis shows that even very expensive thermoelectric materials have the potential to be the most cost effective at the system level, if incorporated with sufficiently short legs and small fill factor. An approximate scaling analysis, verified using numerical calculations, gives the first closed-form, analytical expressions for optimal *L* and *F* to minimize $ per W. The analysis also delineates various cost-dominant regimes with different priorities for materials development, including: (i) a heat exchanger cost dominated regime, where *ZT* should be increased regardless of material or manufacturing costs; (ii) an areal cost, C'', dominated regime at fixed *F*, where ZT/C'' should be maximized, and (iii) a volumetric cost, C''', dominated regime at fixed *F*, where $ZT/(kC''')$ should be maximized, reinforcing the need for low thermal conductivity, *k*. The cost–performance framework derived here will be applied to a number of real materials and applications in a separate manuscript.

Received 1st May 2013
Accepted 18th June 2013

DOI: 10.1039/c3ee41504j

www.rsc.org/ees

Broader context

Thermoelectric devices are attractive for distributed power generation because they convert heat directly into electricity without moving parts. One challenge with thermoelectric power generation is the low efficiency, which is governed in part by the dimensionless figure-of-merit *ZT*. A related problem, addressed here, is the incomplete nature of the *ZT* metric itself which does not consider the heat exchangers or the costs of the thermoelectric generator: the cost of generating power is usually more important than the efficiency alone. This work develops an analytical framework and a new $ per W metric for ranking thermoelectric materials and systems. It is shown that material targets for minimizing $ per W are sometimes, though not always, equivalent to maximizing *ZT*.

1 Introduction

Thermoelectric generators have the potential to be used commercially for electric power generation in a variety of applications, such as distributed solar generation[2] enabled by the development of more efficient solar thermoelectric generators.[3,4] However, the efficiency of most thermoelectric devices is reportedly too low to be competitive with other energy conversion technologies.[5] While efficiency is a useful metric, the cost of generating electricity is more important for the development of commercial devices. This is the case for photovoltaics,[6] where component costs are expressed in the units of $ per W. More sophisticated photovoltaic materials give higher efficiencies resulting in higher power output, but this must be weighed against the increase in capital cost to determine the net effect on the overall system costs and the merits of implementation. The same can be said about thermoelectric generators where the overall system costs, in units of [$ per W] decrease as *ZT* increases, holding all other parameters constant. For this reason, rankings of thermoelectric materials are almost universally given in terms of their *ZT* values. However, *ZT* does not capture device architectures, material costs, manufacturing costs, and the cost of the heat exchangers, all of which strongly influence the overall cost of a thermoelectric generator. These additional factors must be included in any optimization and cost–performance metric before a conclusion is made regarding

[a]*University of California-Berkeley, Department of Mechanical Engineering, 6141 Etcheverry Hall, Berkeley, CA, 94720 USA. E-mail: shannon.yee@berkeley.edu; cdames@berkeley.edu; Fax: +1 51 0642 6163; Tel: +1 51 0642 1338*

[b]*Stanford University, Department of Mechanical Engineering, Building 530, 440 Escondido Mall, Stanford, CA, 94305, USA. E-mail: sleblanc@stanford.edu; goodson@stanford.edu; Fax: +1 65 0723 7657; Tel: +1 65 0725 2086*

[c]*Alphabet Energy, Inc., 26225 Eden Landing Road, Suite D, Hayward, CA, 94545, USA*

† Electronic supplementary information (ESI) available: Fill factor definition, heat exchanger costs, universal axis for Fig. 2, cost-dominant regime map for Fig. 5. See DOI: 10.1039/c3ee41504j

the potential competitiveness of thermoelectric energy conversion and to select the best thermoelectric material for an application.

Several cost analyses for thermoelectrics have been reported previously.[7–10] One earlier analysis considered the cost of fuel for generating heat and concluded that, when heat was essentially free, the thermoelectric generator should be designed to produce maximum power.[7] While this finding is useful, a comprehensive assessment must also consider the material, manufacturing, and heat exchanger costs associated with the system. The cost of the raw materials has also been considered, by comparing the ratio of a material's ZT to its molar specific cost.[10] This approach provides a limited comparison of the cost–performance of various thermoelectric materials because it neglected the device architecture, manufacturing costs, and cost of the heat exchangers which dramatically influence the overall cost–performance.

A third cost analysis focusing on device architecture found a geometric condition that first maximized the areal power density and then explored the system-level costs associated with this power-maximizing geometry.[8] This line of analysis can yield system-level $ per W costs, but has the shortcoming of one-way coupling. The thermoelectric dimensions are optimized strictly for peak power, and this design is then fed into the economic case studies, but the economic problem cannot feed back into the thermoelectric dimensions. Thus, it was not possible to capture additional $ per W improvements by sacrificing some power density for a larger cost savings. This trade-off is especially timely since thermoelectric material performance has recently been improved by the use of potentially expensive nanostructuring techniques.[11,12]

The dominant trend of these prior studies[7–10] is that the system $ per W cost reduces through simultaneous reduction of leg length and fill factor, until such a point that higher-order practicalities (*e.g.*, contact resistances, thermal parasitics, and manufacturability) are no longer negligible. However, we shall see below that ignoring the heat exchanger costs during the optimization[7,8,10] can shift the optimization results by a factor of 5 or more for practical systems. Heat exchanger costs were considered during the optimization in a numerical case study by Kristiansen *et al.*,[9] who found that at the minimal $ per W condition, less than a quarter of the total system cost was due to the thermoelectric material. Importantly, the major results in most prior studies are largely presented in a series of parametric numerical case studies, so there is a current need for compact analytical expressions for the device dimensions that minimize the system level $ per W. In general these are quite different from the well-known optimized dimensions for maximizing efficiency or areal power density.

Here we derive a more comprehensive metric than ZT: the ratio of the thermoelectric system costs to the power generated, denoted by G and with units of [$ per W]. Accurately determining the material, manufacturing, and heat exchanger costs is difficult, and their uncertainties necessarily propagate into G. Nevertheless, this new metric is more meaningful than ZT alone for realistically comparing thermoelectric options. Operating costs, fuel/heat costs, and parasitic heat losses are omitted as beyond the scope of this analysis, but they could be incorporated with suitable generalizations. The analysis reveals a convenient scale for G, given the symbol G_0, which is referred to as the cost–performance metric. G_0 is also shown to be the natural scale for a system's $ per W value when the material costs dominate. In contrast, G describes a system's $ per W value in the more general case when heat exchanger and areal manufacturing costs are also considered. G and G_0 address many of the challenges currently present in ranking materials based solely on ZT or ZT per $ mol^{-1},[10] or optimizing for power per area independently of cost per power.[8] Furthermore, G can also be used to compare thermoelectric systems against other power generation technologies on an overnight capital cost basis. Finally, the cost-minimization, performance-maximization in this manuscript provides the first analytical design framework for a $ per W optimization of thermoelectric leg length and fill factor.

2 Methods

2.1 System-level device physics

To derive the cost–performance metric, we begin with a standard analysis of the device physics of a thermoelectric generator[13] as shown in Fig. 1 for a dual-leg device. We make several common simplifying assumptions: (i) the n- and p-type legs have identical geometries and thermophysical properties (except the Seebeck coefficients which are equal in magnitude but opposite in sign), (ii) the thermal and electrical contact and metallization resistances are negligible, and (iii) the cross-sectional areas of the thermoelectric legs do not vary along their length. Analysis of the thermal circuit in Fig. 1 leads to the dimensionless figure of merit $ZT = S^2\sigma T/k$, which is a combination of the Seebeck coefficient (or thermopower), S [V K^{-1}],

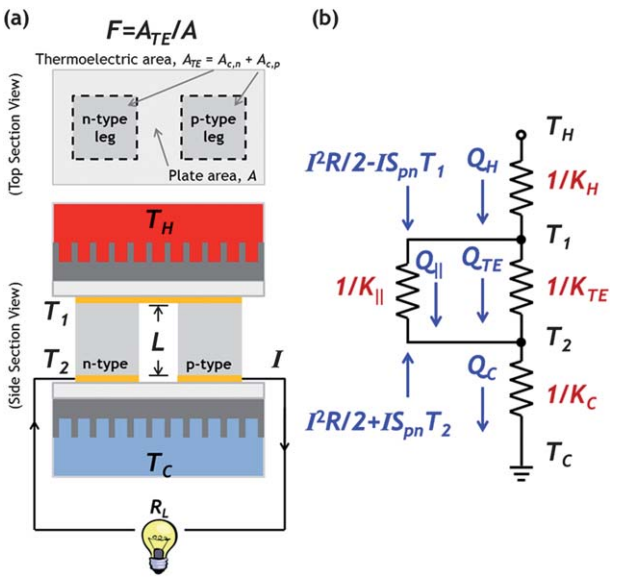

Fig. 1 (a) Two legged thermoelectric device and (b) the equivalent thermal circuit. The internal heat generation term, $I^2R/2$, is the Joule heating component while the Peltier component, $IS_{pn}T$, is responsible for power generation. $K_{||}$ is taken as negligible in the major results below.

the electrical conductivity, σ [S m^{-1}], and the thermal conductivity, k [W m^{-1} K^{-1}], all evaluated at the absolute temperature T [K]. As an additional assumption, (iv) the temperature dependence of S, σ, and k is neglected over the temperature range between the hot- and cold-side of the generator, so Z is independent of T.

Thermoelectric generators can be operated at maximum power or maximum efficiency. In applications where the heat source is essentially free (*e.g.*, solar thermal, nuclear power, or waste-heat recovery), the minimum overall \$ per W cost is achieved by operating at maximum power as confirmed below. On the other hand, when heat is costly (*e.g.*, fossil fuel combustion), operating much closer to the maximum efficiency condition may be preferred. The present analysis will be limited to the former case where heat is abundant/free and therefore the maximum power condition is preferred. In this case for fixed junction temperatures T_1 and T_2, the efficiency is given by[13]

$$\eta_{\mathrm{mp}} = \left(\frac{ZT_1}{ZT_m + ZT_1 + 4}\right)\left(\frac{T_1 - T_2}{T_1}\right) = \eta_{\mathrm{module}}\eta_{\mathrm{Carnot}}, \quad (1)$$

which is a product of the module efficiency, η_{module}, and the Carnot efficiency, η_{Carnot}. Here $T_m = (T_1 + T_2)/2$ is the average temperature of those junctions. If ZT is small, eqn (1) simplifies to

$$\eta_{\mathrm{mp}} \approx \left(\frac{1}{4}\,ZT_1\right)\left(\frac{T_1 - T_2}{T_1}\right). \quad (2)$$

Eqn (2) is an upper bound to the efficiency in eqn (1). The efficiency at maximum power is different from the maximum possible efficiency given by[13]

$$\eta_{\max} = \left(\frac{\sqrt{1 + ZT_m} - 1}{\sqrt{1 + ZT_m} + \frac{T_2}{T_1}}\right)\left(\frac{T_1 - T_2}{T_1}\right). \quad (3)$$

In both cases, operating at either maximum power or maximum efficiency is achieved by varying the electrical load resistance on the generator, R_{L} [Ω], as compared to the internal resistance of the module, R [Ω]. The ratio of these two resistances forms the dimensionless group $m = R_{\mathrm{L}}/R$. When T_1 and T_2 are fixed, power is maximized for $m = 1$, and efficiency for $m = \sqrt{1 + ZT_m}$. If instead it is T_{H} and T_{C} that are fixed, it has recently been noted that m should be somewhat greater than unity even at maximum system power due to thermal feedback from the load resistance affecting the junction temperatures.[8,14,15] Here we use the more conventional[13] load matching condition of $m = 1$ because its modest loss in accuracy is outweighed by its much simpler algebra.

The electrical power, P [W], delivered from a thermoelectric device is simply the product of the heat flowing into the device, Q_{H} [W], and the efficiency, η. An energy balance[8,13] at the hot-side junction in Fig. 1b (*i.e.*, at T_1) gives

$$Q_{\mathrm{H}} = K_{\mathrm{T}}(T_1 - T_2) + S_{\mathrm{pn}}IT_1 - \frac{1}{2}I^2R = K_{\mathrm{H}}(T_{\mathrm{H}} - T_1), \quad (4)$$

where $S_{\mathrm{pn}} = S_{\mathrm{p}} - S_{\mathrm{n}}$ [V K^{-1}] is the junction Seebeck coefficient (the difference in Seebeck coefficients of the p-type and n-type semiconducting legs), K_{T} [W K^{-1}] is the thermal conductance of the device, and K_{H} [W K^{-1}] is the thermal conductance of the hot-side heat exchanger between T_1 and the hot reservoir at T_{H}. Likewise, the heat flowing out of the device is determined by an energy balance at the cold-side junction in Fig. 1b (*i.e.*, at T_2),

$$Q_{\mathrm{C}} = K_{\mathrm{T}}(T_1 - T_2) + S_{\mathrm{pn}}IT_2 + \frac{1}{2}I^2R = K_{\mathrm{C}}(T_2 - T_{\mathrm{C}}), \quad (5)$$

where K_{C} [W K^{-1}] is the thermal conductance of the cold-side heat exchanger. Finally, the electric current flowing through the load and generator can be expressed as

$$I = \frac{S_{\mathrm{pn}}(T_1 - T_2)}{R + R_{\mathrm{L}}} = \frac{S_{\mathrm{pn}}(T_1 - T_2)}{R(m + 1)}. \quad (6)$$

Thus, the electrical power delivered by the generator is

$$P = I^2R_{\mathrm{L}} = \frac{{S_{\mathrm{pn}}}^2(T_1 - T_2)^2}{R}\left(\frac{m}{(m + 1)^2}\right). \quad (7)$$

Since P depends strongly on the junction temperatures and the heat entering the device, the heat exchangers and the thermal conductance of each component are important. These conductances are lumped parameters that also account for the temperature drops across the insulating ceramic plates and any thermal contact resistance present in a real thermoelectric device, which may be worsened or alleviated by the mechanical design considerations of the system. The heat transfer coefficient, U [W m^{-2} K^{-1}], of the heat exchanger describes its conductance through $K = UA$, where A [m^2] is the area of the ceramic plate that joins the thermoelectric generator to the heat exchanger. In many applications the hot- and cold-side heat exchangers have approximately the same heat transfer coefficient, so for simplicity we take $U_{\mathrm{H}} = U_{\mathrm{C}} = U$, $A_{\mathrm{H}} = A_{\mathrm{C}} = A$, and $K_{\mathrm{H}} = K_{\mathrm{C}} = K$ for the remainder of this analysis.

The thermal conductance of the thermoelectric device, $K_{\mathrm{T}} = K_{\parallel} + K_{\mathrm{TE}}$, depends on the conductance of the thermoelectric legs, K_{TE}, and the parallel thermal conductance, $K_{\parallel}$, between legs (*i.e.* due to convection, conduction, and/or radiation across the gap between the plates). These conductances describe the heat flowing through the device which is divided into the portion that conducts through the legs, $Q_{\mathrm{TE}} = K_{\mathrm{TE}}(T_1 - T_2)$, and the portion that goes around the legs, $Q_{\parallel} = K_{\parallel}(T_1 - T_2)$. K_{T} can be expressed as

$$K_{\mathrm{T}} = \frac{k_{\parallel}A(1 - F)}{L} + \frac{k_{\mathrm{p}}AF}{2L} + \frac{k_{\mathrm{n}}AF}{2L} \quad (8)$$

where $F = A_{\mathrm{TE}}/A$ is the fill factor (see Fig. 1a and the ESI†) and L [m] is the thermoelectric leg length. The cross-sectional area of one leg is then $A_{\mathrm{c,n}} = A_{\mathrm{c,p}} = AF/2$ and the legs have thermal conductivities k_{n}, and k_{p}, respectively. The parallel thermal conductance is represented using an equivalent thermal conductivity $k_{\parallel}$, which could also represent linearized radiation and/or natural convection. For simplicity we make the idealization that the heat flowing around the legs is negligibly small (*i.e.*, $K_{\parallel} \ll K_{\mathrm{TE}}$). In practice, more detailed calculations[1,8] show this is valid for most applications with $F > 0.1$ (which defines the lower bound on F for the present analysis) because the thermal

conductance through radiation and the gas is found to be much less than that through the thermoelectric legs. The thermal spreading resistance within the ceramic plates has also been neglected here; this is reportedly a good approximation for $F > 0.01$.[8] For applications with $F < 0.1$ additional measures (*e.g.*, evacuated tubes and radiation management strategies) are used to minimize the thermal leakage conductance. Neglecting $K_{\|}$ for the remainder of this work and taking $k_p = k_n = k$, the module conductance simplifies to

$$K_T \approx \frac{kAF}{L}. \quad (9)$$

Likewise, the electrical resistance of the device is

$$R = \frac{2L}{\sigma_p AF} + \frac{2L}{\sigma_n AF} \approx \frac{4L}{\sigma AF}, \quad (10)$$

under the approximation that the electrical contact resistance and metallization resistances are negligible and $\sigma_p = \sigma_n = \sigma$. This approximation is appropriate as long as $L \gg \sigma R_{c,e}$, where $R_{c,e}$ is the area-specific electrical contact resistance, typically $10^{-9}\ \Omega\ m^2$ for good contacts. Thus, for a typical $\sigma \approx 10^5\ S\ m^{-1}$, a lower bound on L consistent with our neglect of contact resistances is $L > 1$ mm.

Finally, it is useful to define a characteristic thermal length, L_T [m], as

$$L_T \equiv \frac{k}{U}. \quad (11)$$

For $F \approx 1$, when L_T is much larger than the thermoelectric leg length L, the heat exchangers dominate the thermal resistance and temperature drop in the device. This thermal length parameter is a useful normalization condition and will be used as a characteristic length scale for comparison throughout this work. Once a material and an application (including heat exchanger type) are selected, L_T is a known constant.

2.2 Thermal impedance matching

It is important to consider how the temperature drop is distributed through the device. Heat exchangers with high U-values are desirable. With fixed U and F, if the thermoelectric legs are too short, then the temperature drop across the module, and thus the power output, would be small (eqn (7) and (9)). On the other hand, if the thermoelectric legs are too long, then the total thermal resistance also becomes large, reducing Q_H. The electrical resistance would then also be large (eqn (10)). Both effects reduce the power output. Using an intermediate leg length that optimizes this trade-off is referred to as thermal impedance matching.[16] A simplified optimization published previously[15] argued that having about half of the temperature drop occur across the thermoelectric is ideal, while more detailed optimizations suggest corrections to the peak-power leg length of order $(1 + ZT)^{1/2}$ [ref. 16] or $(1 + ZT)^{1/2}(1 + ZT/2)^{-1}$ [ref. 14]. The latter of these is only 6% at $ZT = 1$, and so for simplicity below we ignore such corrections.

We now give a simplified derivation of the thermal impedance matching result, by introducing one of the key analytical approximations to be used later. To motivate this approximation, we note that for a typical application with $T_1/T_2 \approx 2$ and $ZT_1 \approx 1$, from eqn (2) the overall efficiency is $\eta < 13\%$. Therefore, over 87% of the heat entering the device exits the device on the cold-side. Thus, to within accuracy of order η, it can be shown that the heat flows Q_H, Q_{TE}, and Q_C are all approximately equal,

$$K_H(T_H - T_1) \approx K_T(T_1 - T_2) \approx K_C(T_2 - T_C). \quad (12)$$

Then the temperature drop across the module can be expressed simply as

$$T_1 - T_2 \approx \frac{K_H K_C}{K_C K_T + K_H K_T + K_H K_C}(T_H - T_C). \quad (13)$$

The chief benefit of this approximation is the resulting analytical simplicity, which is necessary to obtain the major closed-form results in the remainder of this paper. Eqn (12) and (13) are exact in the limit of small ZT, while for $ZT \approx 1$ introduce errors typically at the level of tens of per cent, as verified below by comparison with selected exact numerical calculations. Further analytical refinement may be possible by accounting for the Peltier and Joule heating terms using an effective thermal conductivity,[3,17] especially for larger ZTs, at the cost of some additional algebraic complexity. However, since the principal goal of the present work is to obtain compact analytical results that incorporate a broad range of thermal and cost phenomena, we elect to sacrifice accuracy at the tens of per cent level in favour of larger gains in simplicity and insight. This is reasonable considering the order-of-magnitude variations in the $ per W metrics that will be seen below.

Because the hot and cold heat exchangers are matched ($K_C = K_H = K = UA$), with the use of eqn (9)–(11) and (13), the power can be expressed as

$$P = \frac{S_{pn}^2 \sigma (T_H - T_C)^2 AF}{4}\left(\frac{m}{(m+1)^2}\right)\left(\frac{L}{(2L_T F + L)^2}\right) \quad (14)$$

with the leg length that maximizes the power being

$$L = 2FL_T. \quad (15)$$

This is the thermal impedance matching condition[15,16] and is referenced as such below. At this condition eqn (13) yields

$$T_1 - T_2 \approx \frac{1}{2}(T_H - T_C), \quad (16)$$

which shows that the maximum power output is obtained when half the temperature drop occurs across the module.

2.3 Power generation cost metric

The present analysis considers overnight capital costs while neglecting operating, maintenance, fuel (*i.e.*, heat is treated as free), and hermetic seal costs. The total cost of a thermoelectric generator system here can be divided into (i) volumetric module costs, (ii) areal module costs, and (iii) heat exchanger costs. The volumetric module costs, C''' [$ per m^3], include the cost of the thermoelectric material, volumetric manufacturing costs (*e.g.*

ball milling and hot pressing), and any other costs that scale with the amount of thermoelectric material. The areal module costs, C'' [\$ per m^2], include the cost of the metallization, areal manufacturing costs (*e.g.*, dicing and cutting), and any other costs that scale with the area of the module. Although many materials have similar C''' and C'', a few (*e.g.* microfabricated nanowires, superlattices grown from molecular beam epitaxy) can have much larger costs due to their specialized manufacturing techniques. While numerical values for C''' and C'' are generally difficult to obtain, they are reported for thirty common thermoelectric materials in a separate manuscript.[1]

The heat exchanger costs, C_{HX}, although rarely considered previously, will in fact turn out to be dominant in many practical situations. Based on engineering handbook data, these costs are typically normalized to their heat transfer coefficient and expressed with units [\$ per W K^{-1}].[18] For a specific class of heat exchangers and ratio of heat load to temperature drop, C_{HX} is constant to a good approximation[18] (see ESI and Fig. S1†). Therefore, the areal cost of the heat exchanger can be expressed as $C_{HX}U$ [\$ per m^2]. For typical real heat exchangers, C_{HX} may range as small as ~\$0.10 per W K^{-1} for MW-scale units, to ~\$10 per W K^{-1} or more for kW-scale and smaller units.[18] Here we use a conservative value of $C_{HX} = 18.48$ \$ per W K^{-1}, which also accounts for the thermal and cost contributions of a standard alumina ceramic plate, and chosen to be consistent with our more extensive study.[1]

In this manner, the total cost of the device, C [\$], can be expressed as

$$C = (C'''L + C'')AF + C_{HX}UA, \quad (17)$$

which scales with the area and fill factor. In this form C'' and C_{HX} are totals accounting for both hot and cold sides, and thus are double the values that would be used for a single plate or a single heat exchanger. Dividing C by the power generated yields the cost G on a [\$ per W] basis. Using eqn (7) and (17), we obtain

$$G = \frac{C}{P} = \frac{4\left((m+1)^2/m\right)}{S_{pn}{}^2\sigma(T_1 - T_2)^2}\left(C'''L^2 + C''L + \frac{C_{HX}UL}{F}\right). \quad (18)$$

Finally, using eqn (13) and matched heat exchangers, the unknown junction temperatures T_1 and T_2 can be eliminated using the known reservoir temperatures T_H and T_C, leading to the approximate result

$$G \approx \frac{4\left((m+1)^2/m\right)}{S_{pn}{}^2\sigma(T_H - T_C)^2}\left(2\frac{K_T}{K} + 1\right)^2\left(C'''L^2 + C''L + \frac{C_{HX}UL}{F}\right). \quad (19)$$

By inspection, the value of m that minimizes G is the load matching condition $m = 1$. Since the heat exchanger is considered a fixed entity during this optimization, this is readily understood as corresponding to maximum power[13] (as noted above, this is an approximation since for finite U peak power occurs at m slightly greater than unity[14,15]). If heat is not free, and fuel costs are significant, then a different optimal load condition will balance the capital cost and fuel costs as discussed elsewhere.[7]

Eqn (18) and the approximate form of eqn (19) are the major new governing equations obtained in this work, and describe the overall cost–performance of the thermoelectric system. These equations also allow for direct comparisons between thermoelectric power generation and other electricity generation technologies on the same \$ per W basis. The approximations in eqn (13) and (19) will always over-predict the actual temperature difference and power generated. Therefore, the approximate G from eqn (19) will always be less than the exact value from eqn (18), making eqn (19) a lower (*i.e.* optimistic) bound for the \$ per W cost of a thermoelectric system.

3 Results and discussion

3.1 Non-dimensionalization

G captures the coupled economic and thermal–electrical nature of the technology. To provide additional insight we simplify the analysis using non-dimensionalization and scaling arguments. Analytical forms are also desirable for their greater universality and adaptability as compared to primarily numerical case studies based on selected scenarios.[7–9] First, it is necessary to identify the pertinent dimensionless groups, summarized in Table 1. In many applications the heat exchangers (and therefore the U-value) and the thermoelectric material (and therefore k) are pre-selected and held as design constants. As a result the thermal length L_T (eqn (11)) is often fixed, so we adopt it as the main normalizing factor, indicated with an over-tilde. The first dimensionless group is

$$\tilde{L} \equiv \frac{L}{L_T} = \frac{UL}{k}, \quad (20)$$

which can also be referred to as a device Biot number. This group quantifies the distribution of the temperature drops in the device. At the thermal impedance matching condition, $\tilde{L} = 2F$. For $\tilde{L} > 2F$, the temperature drop is primarily across the module while, for $\tilde{L}$ less than this, the temperature drop is primarily across the heat exchangers.

Table 1 Summary of key dimensional and non-dimensional quantities

	Module length	Module areal cost	Heat exchanger cost
Dimensional [m]	$L,\ L_T \equiv \frac{k}{U}$	$L_C \equiv \frac{C''}{C'''}$	$L_{HX} \equiv \frac{C_{HX}U}{C'''}$
Non-dimensional	$\tilde{L} \equiv \frac{L}{L_T} = \frac{UL}{k}$	$\tilde{L}_C \equiv \frac{L_C}{L_T} = \frac{C''}{C'''}\frac{U}{k}$	$\tilde{L}_{HX} \equiv \frac{L_{HX}}{L_T} = \frac{C_{HX}U}{C'''}\frac{U}{k}$

Another useful length scale is the module cost length, L_C [m], defined as the ratio of the module's areal and volumetric costs

$$L_C \equiv \frac{C''}{C'''}. \quad (21)$$

Referring to the total cost in eqn (17), when $L_C \gg L$ the module's volumetric costs can be neglected. When $L_C \ll L$ the module's areal costs can be neglected. L_C can be normalized by L_T to form another helpful group,

$$\tilde{L}_C \equiv \frac{L_C}{L_T} = \frac{C''}{C'''}\frac{U}{k}. \quad (22)$$

Finally, the last useful length is the ratio of the heat exchanger areal cost to the module volumetric cost, termed the heat exchanger cost length, L_{HX} [m]

$$L_{HX} \equiv \frac{C_{HX}U}{C'''}. \quad (23)$$

Referring to eqn (17), when $L_{HX} \ll LF$, the heat exchanger costs can be neglected compared to the module's volumetric costs. When $L_{HX} \gg LF$, the heat exchanger cost dominates the module's volumetric costs. Normalizing to L_T gives the dimensionless group

$$\tilde{L}_{HX} \equiv \frac{L_{HX}}{L_T} = \frac{C_{HX}U}{C'''}\frac{U}{k}. \quad (24)$$

These three dimensionless groups help simplify eqn (18) and (19). To proceed with an exact solution, the temperature drop across the thermoelectric legs (*i.e.*, $T_1 - T_2$) can be solved numerically from the non-linear system eqn (4) and (5).[1] However, to retain analytical insight with only a modest loss of accuracy, we proceed by invoking the same approximations used in eqn (13). As discussed earlier, this approximation gives a lower bound on the costs. With the help of eqn (19)–(24), the cost can now be expressed as a product of dimensionless groups

$$\frac{G}{G_0} \approx \frac{1}{4}\left(\frac{(m+1)^2}{m}\right)\left(2F + \tilde{L}\right)^2\left(1 + \tilde{L}_C\frac{1}{\tilde{L}} + \frac{\tilde{L}_{HX}}{\tilde{L}F}\right), \quad (25)$$

where

$$G_0 = \frac{16C'''{L_T}^2}{{S_{pn}}^2\sigma\left(T_H - T_C\right)^2}. \quad (26)$$

$\tilde{L}_C$ and $\tilde{L}_{HX}$ are understood to be constants once a material and heat exchangers have been selected.

The parameter G_0 has units of [\$ per W], and is one natural cost–performance scale for G. G_0 as defined in eqn (26) incorporates the material cost, application temperatures, heat exchanger thermal performance, and thermoelectric material properties. Ultimately, it is always G rather than G_0 that should be minimized and used to compare different power generation technologies. We shall see below that the scaling relationship between G_0 and the minimal G can vary depending on certain constraints of the system being analysed. For example, in the general case allowing for all three cost phenomena of eqn (17), $G_{min} = 8G_0\tilde{L}_{HX}$. On the other hand, when only the material costs are considered and F is fixed while L is optimized, $G_{min} = 4G_0F^2$, and thus in this case G_0 directly measures the system's cost–performance. In general the values for G_{min} and G_0 can differ by an order of magnitude; G_0 represents only the material cost while G_{min} always represents the entire system cost.

While G_0 arose naturally from the mathematics, it can also be recast in a more intuitive form

$$G_0 = \frac{C'''L_TA}{\frac{1}{4}ZT_H\left(\frac{T_H - T_C}{T_H}\right)}\frac{1}{UA(T_H - T_C)}. \quad (27)$$

This form is readily seen to be the natural scale for G of a thermally impedance matched system ($L = 2L_T$) with $F = 1$ and dominated by the material's volumetric costs. For such a system, the numerator of the first term represents the material cost, while the denominator of the first term is a scale for the system efficiency in the small ZT limit (eqn (2)). Furthermore, the denominator of the second term gives a measure of the heat flow [W] that can be delivered by this application. To achieve small G_0, a low volumetric cost and low thermal conductivity are necessary. The device must also have large ZT and therefore high efficiency. Finally, the heat exchangers should have large U-values in order to allow for large thermal power density.

3.2 Cost–performance optimization

We now consider the minimization of G with respect to the design parameters m, L, and F, emphasizing analytical results. The m optimization is trivial because eqn (19) and (25) are minimized for $m = 1$. But what are the optimal values of L and F? To answer this question, Fig. 2 depicts a G-surface as a function of F and L. Although Fig. 2 was generated using realistic properties based on a Bi_2Te_3 application, the figure can also be recast in a much more universal form using material-independent axes which are motivated in the ESI.†

Fig. 2 shows there is no global minimum in the $G(\tilde{L},F)$ function, excluding the impractical $\tilde{L} = 0$ and $F = 0$ point where there is no device (and contact resistances would no longer be negligible anyway). However, there is a trough along the thermal impedance matching line $2F = \tilde{L}$. As $\tilde{L}$ or F approaches zero, G approaches $8G_0\tilde{L}_{HX}$. This trough results from a competition between cost and thermoelectric performance. As the device is made thinner (smaller L at constant F), or the leg density more sparse (smaller F at constant L), less material is used, thus reducing the cost. However, decreasing $\tilde{L}$ at fixed F also reduces the temperature drop across the device, resulting in less electrical power generated. Similarly, as the device is made sparse (smaller F, fixed L), the internal electrical resistance increases (eqn (10)), and less electrical power is generated. This is an example of the trade-off between cost and power output: a lower power device may be preferred if the cost savings are good enough on a \$ per W basis.

While there is no minimum in G, crucially there is a point of diminishing returns at *finite* L and F. This is a characteristic point below which further decreasing L or F has only marginal benefit, and this point will be discussed more fully in Section 3.5. First, consider minimizing G with respect to F while holding L fixed. After solving $\left.\frac{\partial G}{\partial F}\right|_L = 0$, the resultant condition on F is the solid blue line in Fig. 2 given as

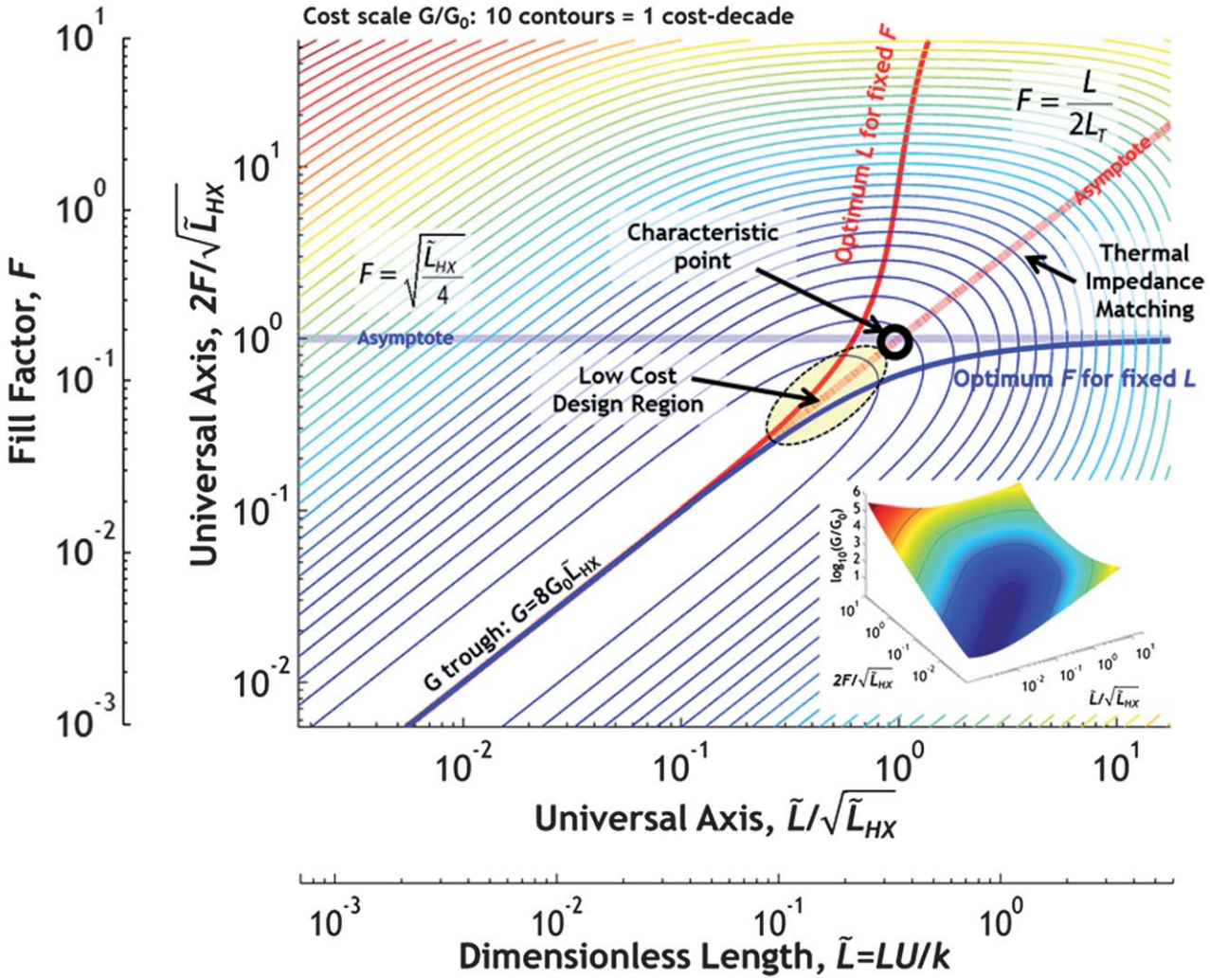

Fig. 2 Example cost-design field for Bi_2Te_3.[19,20] This figure was calculated for a specific application of Bi_2Te_3 (outer pair of axes). As discussed in the text, this G surface can also be expressed in a material-independent form using scaled universal axes (inner pair). The parameters are: $S_{pn} = 464\ \mu V\ K^{-1}$, $\sigma = 682\ S\ cm^{-1}$, $k = 1.57\ W\ m^{-1}\ K^{-1}$, $C''' = \$0.89\ cm^{-3}$, $C'' = \$0.017\ cm^{-2}$, $C_{HX} = \$18.48$ per $W\ K^{-1}$, $U = 100\ W\ m^{-2}\ K^{-1}$, $T_H = 100\ °C$, $T_C = 20\ °C$. The contours represent lines of constant G/G_0 as given by the surface in the inset. For fixed F, optimizing G with respect to L gives the dark red curve; likewise, optimization at fixed L gives the dark blue curve. Both converge at low F and L. The characteristic point is taken as the intersection of the two asymptotes (light lines). The low cost design region is along the thermal impedance matching line $F = L/(2L_T)$ but below the characteristic point; there is little further benefit in G if F and L are decreased further.

$$F_{opt} = \frac{\sqrt{\tilde{L}_{HX}^{\ 2} + 4\tilde{L}_{HX}\tilde{L}_C\tilde{L} + 4\tilde{L}_{HX}\tilde{L}^2} - \tilde{L}_{HX}}{4\left(\tilde{L}_C + \tilde{L}\right)}. \qquad (28)$$

For small and large L this can be approximated as

$$\begin{aligned} L \to 0 &: F_{opt} = \frac{L}{2L_T} \underset{m=1}{\Rightarrow} G|_{F=F_{opt}} \approx 8G_0\,\tilde{L}_{HX} \\ L \to \infty &: F_{opt} = \sqrt{\frac{\tilde{L}_{HX}}{4}} \underset{m=1}{\Rightarrow} G|_{F=F_{opt}} \approx G_0\left(\frac{L}{L_T}\right)^2. \end{aligned} \qquad (29)$$

Similarly, minimizing G with respect to L for fixed F gives the solid red line in Fig. 2 and

$$L_{opt} = \frac{4FL_T\sqrt{F\tilde{L}_C + \tilde{L}_{HX}}}{\sqrt{F\tilde{L}_C + \tilde{L}_{HX}} + \sqrt{\left(F\tilde{L}_C + \tilde{L}_{HX}\right) + 16F^2}}, \qquad (30)$$

which can be approximated for small and large F as

$$\begin{aligned} F \to 0 &: L_{opt} = 2L_T F \underset{m=1}{\Rightarrow} G|_{L=L_{opt}} \approx 8G_0\tilde{L}_{HX} \\ F \to \infty &: L_{opt} = L_T\sqrt{F\tilde{L}_C} \underset{m=1}{\Rightarrow} G|_{L=L_{opt}} \approx 4G_0F^2. \end{aligned} \qquad (31)$$

The two optimum conditions (eqn (28) and (30)) converge at low values of L and F along the design condition

$$2F = \frac{L}{L_T} = \tilde{L}, \qquad (32)$$

which is exactly the thermal impedance matching condition in eqn (15) and the light red line in Fig. 2. Under this condition and the load matching condition $m = 1$, eqn (25) simplifies to

$$\left.\frac{G}{G_0}\right|_{\tilde{L}=2F} \approx 4\left(4F^2 + 2\tilde{L}_C F + 2\tilde{L}_{HX}\right), \qquad (33)$$

or equivalently

$$\left.\frac{G}{G_0}\right|_{F=\frac{\tilde{L}}{2}} \approx 4\left(\tilde{L}^2 + \tilde{L}_C\tilde{L} + 2\tilde{L}_{HX}\right), \quad (34)$$

which shows G as a direct function of either F or L (the latter through $\tilde{L} = L/L_T$). These forms are useful because they highlight the benefit of reducing F and L together to minimize G, and also the diminishing returns nature where only the HX costs remain. The three terms in eqn (33) and (34) can be tracked back to eqn (19). The first term represents the module volumetric cost, the second term represents the module areal cost (*i.e.*, $\tilde{L}_C \propto C''$), and the third term represents the heat exchanger cost (*i.e.*, $\tilde{L}_{HX} \propto C_{HX}$).

3.3 Example calculation for Bi_2Te_3

To illustrate this new framework, we present an example calculation for Bi_2Te_3 using the material and application properties given in the caption of Fig. 2. This same analysis is applied to thirty materials and four different applications in a separate manuscript.[1] To quantify the impact of the approximation from eqn (13), we compare the exact (eqn (18): numerical) and approximate (eqn (19): analytical) calculations. We consider a fixed fill factor of $F_{opt} = 0.18$, whose origin will be shown later in eqn (38). At this F, eqn (30) gives an optimum leg length of $L_{opt} = 3.5$ mm, and eqn (19) returns a minimum cost of $G = \$55.45$ per W. For this same fill factor of 0.18, the exact analysis (eqn (18)) can be evaluated using the exact junction temperatures. This numerical solution now gives $L_{opt} = 4.5$ mm and a minimum cost of $G = \$97.64$ per W. While these \$ per W values may appear large, they incorporate the entire system cost including a specified heat exchanger (with $U = 100$ W m^{-2} K^{-1} at a conservative cost of $C_{HX} = \$18.48$ per W K^{-1}). The scenario of a free heat exchanger will yield much smaller \$ per W values and is presented later. Furthermore, this scenario has a very modest reservoir temperature difference of 80 °C, and G scales as $(T_H - T_C)^{-2}$.

The calculations just given confirm that the approximate cost always under predicts the exact calculation, providing a lower (*i.e.*, optimistic) bound for what is achievable. This level of agreement between approximate and exact analyses is typical for materials with $ZT \sim 1$, and we have confirmed that the two analyses converge as $ZT \to 0$, consistent with the discussion around eqn (12). The dominant source of error is the approximation of eqn (13); using a $k_{eff} \approx k(1 + 0.395ZT)$ [ref. 17] to correct the approximate leg length implies $L_{opt} \approx 4.6$ mm, now very close to the exact numerical value. This agreement to within tens of per cent confirms that the analytical simplifications made above are reasonable and prove helpful both for physical insight and for rapid screening of candidate materials and systems.

As long as L_{opt} and F_{opt} are practically achievable for the application, the total cost is limited only by the heat exchanger, and this design would approach the best possible \$ per W given the input parameters (see also the flowchart in Fig. S2†). On the other hand, if these calculated values of L_{opt} and/or F_{opt} are considered impractically small (*e.g.*, due to manufacturability, mechanical robustness, non-negligible contact resistances or thermal parasitics, *etc.*), then the optimization should be repeated with the minimum allowable L and/or F (see heavy blue and/or red lines in Fig. 2), and the cost contributions from C'' and/or C''' can no longer be neglected in the final design.

3.4 Special case: "free" heat exchanger and prescribed F

In some cases it may be judged appropriate to exclude the cost of the heat exchangers when performing the overall \$ per W optimization. For example, the cost of the heat exchangers might plausibly be excluded when incorporating thermoelectric power generation into a solar hot water heater since the heat exchanger hardware already exists. This scenario is also common in prior reports and is instructive because it isolates the cost of only the thermoelectric module. However, the reader is cautioned that even a small heat exchanger cost can have a dramatic effect on the system optimization, including L_{opt}, F_{opt}, and G_{min}, so proper cost accounting is essential.

In this special case, the third term in the cost equation can be dropped, and eqn (25) reduces to

$$\frac{G}{G_0} \approx \frac{1}{4}\left(\frac{(m+1)^2}{m}\right)\left(2F + \tilde{L}\right)^2\left(1 + \frac{\tilde{L}_C}{\tilde{L}}\right). \quad (35)$$

In contrast to eqn (25) and Fig. 2, eqn (35) does not exhibit an optimum or even a diminishing returns region in its $G(\tilde{L},F)$ surface. We focus on situations where the value of F is fixed. For example, F can be fixed by some other practical constraint excluded from the above analysis (*e.g.*, mechanical robustness, parasitic heat losses, manufacturability, *etc.*), or it can be fixed to the asymptotic value in Fig. 2. Holding F fixed and optimizing for L yields

$$L_{opt} = \frac{4L_T F}{1 + \sqrt{1 + 16F/\tilde{L}_C}}, \quad (36)$$

which is a simplification of eqn (30) with $\tilde{L}_{HX} = 0$. This optimum leg length produces the best cost–power trade-off for a fixed F and "free" heat exchanger. Making the leg length longer than this increases the cost C. Making the legs shorter, while reducing C, reduces the temperature drop across the module and therefore decreases the power.

In this fixed-F condition the limiting behaviour for large and small $\tilde{L}_C$ is

$$\begin{aligned} &\tilde{L}_C \gg 16F : L_{opt} = 2L_T F \underset{m=1}{\Rightarrow} G|_{L=L_{opt}} \approx 8G_0F\tilde{L}_C \\ &\tilde{L}_C \ll 16F : L_{opt} = L_T\sqrt{F\tilde{L}_C} \underset{m=1}{\Rightarrow} G|_{L=L_{opt}} \approx 4G_0F^2 \end{aligned} \quad (37)$$

In the large $\tilde{L}_C$ limit, the thermal impedance matching condition is recovered: since the total cost is dominated by the C'' term, there is no additional cost penalty in setting L equal to the full thermal-impedance-matched value to maximize power. In the small $\tilde{L}_C$ limit, L_{opt} is the geometric mean of FL_T and L_C, which reflects the compromise between thermal efficiency and cost. In this case, a smaller G is achieved by reducing L well below the thermal-impedance-match value of $2FL_T$, but the reduction in power is more than offset by the reduction in cost. The optimum leg length and cost results of eqn (35) and (36),

along with their asymptotic approximations from eqn (37), are shown in Fig. 3 in non-dimensional form. Consistent with the criteria of eqn (37), the transition between these extremes happens around $L_C \approx FL_T$ (that is, $\tilde{L}_C \approx F$).

For most currently available materials and manufacturing processes, a detailed survey shows that $\tilde{L}_C$ typically ranges between 0.001 and 0.1 (shaded region in Fig. 3).[1] Practical values of F also range widely, from close to unity down to ~0.01.[8] Therefore, eqn (37) shows the small $\tilde{L}_C$ limit is most common.

Thus, if the heat exchanger cost is ignored, $ per W minimization in real systems will typically result in an optimal leg length far smaller than the traditional thermal impedance matched condition. For example, a typical case with $\tilde{L}_C = 0.01$ and $F = 0.1$ should use an L_{opt} over 6 times shorter than $2FL_T$. This is an essential example of the cost–performance trade-off. We note that this effect cannot be captured by sequential analyses that optimize for power density before costs.[8]

Finally, the dimensionless results are recast in dimensional form (Fig. 4) to help graphically determine the optimum leg length for the case $F \approx 1$ (eqn (36)). The shaded regions are the domains where typical materials, costs, and applications reside.[1] The red line indicates the asymptotic behaviour for a system dominated solely by areal costs (*i.e.*, inexpensive thermoelectric material). With the cost length, L_C, and the thermal length, L_T, for a specific material–application combination, the optimum leg length can be determined from this plot.

Returning to the example of Bi_2Te_3, in this special case of a "free" heat exchanger with a chosen fill factor of $F = 0.18$, the approximate solution (eqn (35)) gives $G = \$7.90$ per W (with $L = 0.69$ mm). This is also in reasonably good agreement with the exact numerical solution which gives $G = \$14.63$ per W (with $L = 0.77$ mm). These costs are quadratically sensitive to $T_H - T_C$ through G_0 (eqn (26)), and thus can be improved substantially by increasing the reservoir temperature difference beyond the modest value of 80 °C used here. Most importantly, the L and G values obtained here for a free heat exchanger are all at least 5× smaller than those found in Section 3.3 for a realistic heat exchanger cost of $18.48 per W K^{-1}. These large differences again emphasize the major impact that the heat exchanger costs have on both geometry and costs for a thermoelectric power generator.

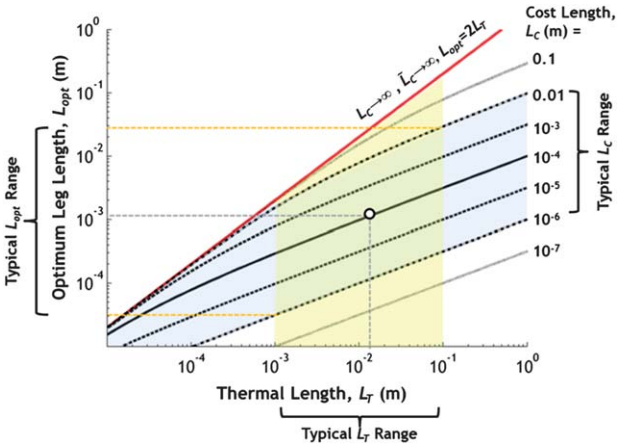

Fig. 4 Optimum thermoelectric leg length as a function of L_T for various L_C, for the special case of a free heat exchanger and $F = 1$. This is a dimensional representation of Fig. 3a. Using these curves, the optimum length of the thermoelectric leg can be determined graphically. The data point corresponds to a Bi_2Te_3 application with the same properties as in Fig. 1. The uppermost red line corresponds to the traditional thermal impedance matching condition, but this figure shows that L_{opt} for realistic materials and applications will generally be much smaller.

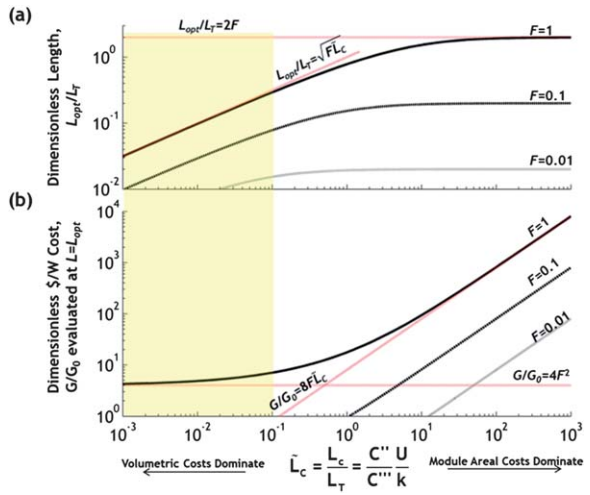

Fig. 3 Dimensionless cost analysis for the special case of a "free" heat exchanger. (a) The dimensionless optimum length and (b) dimensionless $ per W cost evaluated at the optimum length, both given as functions of F and the dimensionless parameter $\tilde{L}_C$. For most realistic materials and applications, $\tilde{L}_C$ typically ranges between 0.001 and 0.1 (shaded region), in which case the cost considerations force the optimal leg length to be well below the usually assumed thermal impedance matching condition.

3.5 Characteristic point, universal axes, and limiting forms

As shown in Fig. 2, G/G_0 decreases with decreasing F and $\tilde{L}$ along the thermal impedance matching line $\tilde{L} = 2F$. As a characteristic point representing the transition to diminishing returns, we take the intersection of the light red and blue lines in Fig. 2 which returns the coordinate

$$\frac{L_{opt}}{L_T} = \sqrt{\tilde{L}_{HX}},\ F_{opt} = \sqrt{\frac{\tilde{L}_{HX}}{4}}. \quad (38)$$

Although this is not a true optimum, the shorthand "opt" is used for convenience. Alternatively, using the universal axes given in the figure, this is exactly the coordinate (1,1), which is valid for most realistic materials and heat exchangers (see ESI†). In the Bi_2Te_3 example of Fig. 2, the diminishing returns point is $L_{opt} = 5.7$ mm and $F_{opt} = 0.18$. Crucially, these numerical values are well within the range of practicality. This confirms the appropriateness of this derivation's key assumptions, including neglecting contact resistances and parallel heat leakage ($K_{||}$). Eqn (38) shows how the optimal system design depends strongly on the costs of both material and heat exchanger, *via* $\tilde{L}_{HX}$.

We now consider three limiting behaviours (Fig. 5) determined by which cost term dominates eqn (17). The most general case allows for finite heat exchanger costs. At the coordinates of eqn (38), $G/G_0 \approx 12\tilde{L}_{HX}$, which is 50% greater

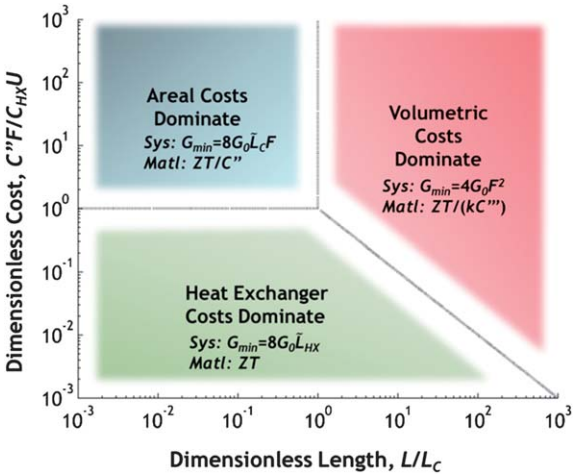

Fig. 5 Simplified regime map showing which component of eqn (17) dominates the overall system cost. Also indicated in each sector are algebraic expressions for its minimum G and the corresponding material-specific quantity to maximize. The expressions obtained for the areal and volumetric sectors assumed fixed F and arbitrary L, while different constraints would give different expressions and materials guidelines. In the best case it is practical to make both F and L sufficiently small that the only remaining cost is that of the heat exchanger, consistent with the trough of Fig. 2.

than the ultimate best-case trough value of $8\tilde{L}_{HX}$ (eqn (29) and (31)). The physical significance of this limit is understood by expanding it as

$$G = 8G_0\,\tilde{L}_{HX} = 8\,\frac{C_{HX}UA}{\frac{1}{4}ZT_H\left(\frac{T_H - T_C}{T_H}\right)UA(T_H - T_C)}. \qquad (39)$$

The numerator is within a numerical constant of the heat exchanger cost, which is the dominant cost in this limit. As long as the application and manufacturing constraints are amenable to having sufficiently small F and L, it is possible to design the thermoelectric generator such that the module costs are negligible and only the heat exchanger costs remain. To make the costs as small as reasonably achievable, L and F should be set to values below eqn (38) subject to the condition $2F = L/L_T$. For example, G can be improved to within 12.5% of the best-case trough value by reducing F and L both by another factor of two. However, F and L cannot be reduced without bound because manufacturing limitations, mechanical robustness, contact resistance issues, and thermal parasitics will eventually become important.

Next, we consider the special case where the heat exchanger cost is neglected ($\tilde{L}_{HX} \to 0$), and F is fixed at some minimum value as in Section 3.4. This leads to two sub-cases (eqn (37)), depending on the trade-off between volumetric and areal costs. When the minimum allowed value of F is small (compared to $\tilde{L}_C/16$), the areal cost dominates and

$$G = 8G_0\tilde{L}_CF = 8\,\frac{C''AF}{\frac{1}{4}ZT_H\left(\frac{T_H - T_C}{T_H}\right)UA(T_H - T_C)}. \qquad (40)$$

Here F should be made as small as practical, followed by setting $L = 2FL_T$.

A third regime exists where the module volumetric costs (*i.e.*, material costs) dominate. In this second subcase, for fixed F large compared to $\tilde{L}_C/16$, the volumetric cost dominate and

$$G = 4G_0F^2 = 2\,\frac{C'''V}{\frac{1}{4}ZT_H\left(\frac{T_H - T_C}{T_H}\right)UA(T_H - T_C)} \qquad (41)$$

where the numerator is the volumetric cost of a module with (equivalent) volume $V = (AF)(2FL_T)$. A corresponding expression for fixed L and variable F can be obtained by replacing $F \to LU/2k$ in eqn (41).

There are a number of limiting conditions depending on which cost term dominates eqn (17) and whether there are any practical constraints limiting F and/or L. The three cases considered here are for: (i) when heat exchanger costs dominate (eqn (39)), (ii) free heat exchangers, fixed F, and areal manufacturing costs dominate (eqn (40)), and (iii) free heat exchangers, fixed F, and material costs dominate (eqn (41)). It is noteworthy that eqn (39), (40), and (41) all take a similar form with the numerator representing each regime's dominant cost. Knowing the dominant costs provides useful feedback to designers regarding what changes could have the greatest reduction in cost. This comparison is summarized in the cost-dominant regime map of Fig. 5 (see also ESI†). The horizontal axis gives the ratio of volumetric to areal costs, and the vertical axis is the ratio of areal and heat exchanger costs. The diagonal line represents the comparison between volumetric costs and heat exchanger costs. Finally, at (1,1) all three costs are equal. Fig. 5 allows for graphical determination of the dominant cost, and it can quickly provide the relative cost breakdown for a given design.

4 Conclusions

This work derives new system-level cost metrics G with units of [$ per W], for thermoelectric power generation when heat is free. These metrics go beyond ranking materials by ZT per $ per mol (ref. 10) or sequential optimization of power prior to cost,[8] by using a coupled co-optimization to account for heat exchangers, areal manufacturing (C''), and volumetric material (C''') costs. A natural scale for G is found to be G_0, which can be understood as describing the material cost part of G, analogous to how the material ZT is useful in describing the module ZT.

Closed-form analytical expressions are obtained for the optimum thermoelectric leg length and module fill factor that minimize G, and reflect an inherently coupled trade-off between cost and thermoelectric performance. The simple analytical results for L_{opt} and F_{opt} are exact in the limit of small ZT, and remain accurate to within tens of per cent for $ZT \sim 1$. Several cost-dominant regimes have been identified, as summarized in Fig. 5: (i) a heat exchanger cost dominated regime, where $G_0\tilde{L}_{HX}$ should be minimized; (ii) a module areal manufacturing cost dominated regime, where at constrained F, $G_0\tilde{L}_CF$ should be minimized; and (iii) a volumetric material cost dominated regime, where at constrained F, G_0F^2 should be minimized.

Focusing specifically on recommendations for manufacturing and materials development, the relevant material figures-of-merit which should be maximized in each regime are (i) ZT regardless of cost; (ii) the ratio ZT/C''; and (iii) the ratio $ZT/(kC''')$.

Importantly, it is shown that ignoring the heat exchanger costs can shift the optimized values of L, F, and G by a factor of 5 or more. A realistic Bi_2Te_3 case study yields the important conclusion that it is indeed practical to reduce L and F to the diminishing returns point whereby the total costs are dominated by the heat exchanger (*i.e.*, regime (i)). A detailed investigation[1] of thirty real materials and four applications shows that this is broadly the case.

This analytical framework is helpful for rapid projections and scaling. Referring to the baseline Bi_2Te_3 case study of Fig. 2, the C_{HX} for installations at large scale[18] might plausibly be reduced by a factor of nine, to \$2.05 per W K^{-1}. Thus, eqn (38) shows that the target L and F values at the head of the trough will both be reduced by factors of three, to 1.9 mm and 0.061, and we quickly conclude that it should still be practical to design for regime (i). Furthermore, if the reservoir temperature difference is increased by a factor of 4 (to 320 °C), we immediately see that $G_{min} \approx 12G_0\tilde{L}_{HX}$ at the head of the trough will be reduced by a factor of 144. This would represent a tremendous improvement from G_{min} = \$59.3 per W to \$0.41 per W, and suggests that thermoelectrics may indeed have the potential to be cost competitive with other technologies for large-scale power generation.[1]

Acknowledgements

S. K. Yee would like to acknowledge support from the John and Fannie Hertz Foundation Fellowship and the Big George Fellowship. S. LeBlanc would like to acknowledge the Sandia National Lab Fellowship and the Stanford DARE Fellowship. S. LeBlanc and K. Goodson gratefully acknowledge funding support through the NSF/DOE Partnership on Thermoelectric Devices for Vehicle Applications (Grant no. 1048796). C. Dames is grateful for support from the NSF (Grant no. 1055317). We would also like to thank Profs Arun Majumdar, Gang Chen, and G. Jeffrey Snyder for insightful discussions.

Notes and references

1 S. LeBlanc, S. K. Yee, M. L. Scullin, C. Dames and K. E. Goodson, 2013, submitted.
2 J. Karni, *Nat. Mater.*, 2011, **10**, 481–482.
3 L. L. Baranowski, G. J. Snyder and E. S. Toberer, *Energy Environ. Sci.*, 2012, **5**, 9055–9067.
4 D. Kraemer, B. Poudel, H.-P. Feng, J. C. Caylor, B. Yu, X. Yan, Y. Ma, X. Wang, D. Wang, A. Muto, K. McEnaney, M. Chiesa, Z. Ren and G. Chen, *Nat. Mater.*, 2011, **10**, 532–538.
5 C. B. Vining, *Nat. Mater.*, 2009, **8**, 83–85.
6 D. M. Powell, M. T. Winkler, H. J. Choi, C. B. Simmons, D. B. Needleman and T. Buonassisi, *Energy Environ. Sci.*, 2012, **5**, 5874.
7 D. M. Rowe and G. Min, *IEE Proc.: Sci., Meas. Technol.*, 1996, **143**, 351–356.
8 K. Yazawa and A. Shakouri, *Environ. Sci. Technol.*, 2011, **45**, 7548–7553.
9 N. R. Kristiansen, G. J. Snyder, H. K. Nielsen and L. Rosendahl, *J. Electron. Mater.*, 2012, **41**, 1024–1029.
10 G. G. Yadav, J. A. Susoreny, G. Zhang, H. Yang and Y. Wu, *Nanoscale*, 2012, **3**, 3555–3562.
11 C. J. Vineis, A. Shakouri, A. Majumdar and M. G. Kanatzidis, *Adv. Mater.*, 2010, **22**, 3970–3980.
12 M. Zebarjadi, K. Esfarjani, M. S. Dresselhaus, Z. F. Ren and G. Chen, *Energy Environ. Sci.*, 2012, **5**, 5147–5162.
13 S. W. Angrist, *Direct Energy Conversion*, Allyn and Bacon, Inc, Boston, 1965.
14 D. M. Rowe, *Thermoelectrics Handbook*, CRC Press, 2006, section 9.6.4 by G. J. Snyder.
15 P. M. Mayer and R. J. Ram, *Nanoscale Microscale Thermophys. Eng.*, 2006, **10**, 143–155.
16 K. Yazawa and A. Shakouri, *J. Appl. Phys.*, 2012, **111**, 024509.
17 L. Baranowski, J. Snyder and E. Toberer, *J. Appl. Phys.*, 2013, **113**, 204904.
18 R. K. Shah and D. P. Sekulic, *Fundamentals of Heat Exchanger Design*, John Wiley & Sons, Hoboken, NJ, 2003.
19 N. D. Lowhorn, W. Wong-Ng, Z.-Q. Lu, J. Martin, M. L. Green, J. E. Bonevich, E. L. Thomas, N. R. Dilley and J. Sharp, *J. Mater. Res.*, 2011, **26**, 1983–1992.
20 W. J. Parker and R. J. Jenkins, *Thermal Conductivity Measurements on Bismuth Telluride in the Presence of a 2 MeV Electron Beam*, Report: USNRDL-TR-462, NSA-15–004387, 1960.